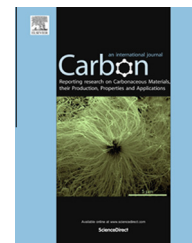


Available at www.sciencedirect.com

ScienceDirect

journal homepage: www.elsevier.com/locate/carbon

Role of the cathode deposit in the carbon arc for the synthesis of nanomaterials

J. Ng ^{*}, Y. Raiteses

Princeton Plasma Physics Laboratory, P.O. Box 451, Princeton, NJ 08543, USA

ARTICLE INFO

Article history:

Received 4 November 2013

Accepted 4 May 2014

Available online 14 May 2014

ABSTRACT

The atmospheric pressure carbon arc in helium is an important method for the production of nanomaterials. Typical arcs operate in a dc mode between a graphite anode, which is consumed, and a cathode which may be a lower melting point material. During arc operation, a carbon deposit is formed on the cathode surface. This deposit may contain different forms of the synthesised fullerenes. It is shown that this deposit plays a crucial role in conducting the arc current. Temperature measurements demonstrate that a sufficiently large area of the cathode deposit is hot enough for thermionic emission to be the source of most of the arc current. Due to the deposit's low thermal conductivity, the cathode behind the deposit does not reach its melting point. The role of the deposit in emitting electrons can probably be generalized for other arc synthesis methods with consumed anodes.

© 2014 Elsevier Ltd. All rights reserved.

1. Introduction

Since their discovery in the early 19th century [1], carbon arcs have been used as radiation standards [2], in image furnaces [3] and in carbon arc welding among other things. More recently, they have been used as an efficient method for the production of high purity carbon nanotubes [4–6], in which the graphite anode ablates and nanotubes and other fullerenes are formed in a carbon deposit on the cathode surface [5,7]. Due to their unique electrical and mechanical properties [8–10], nanotubes could potentially be used for hydrogen storage, nanoelectronics, chemical sensors and many other applications [9,8,11].

Although the initial discovery of nanotubes used graphite for both cathode and anode [4], and this setup is commonly used [5,12,13], Colbert et al. [7] found that using a water cooled copper cathode reduced sintering in the nanotubes formed in the deposit, while other workers have used cathodes of materials such as copper and stainless steel [14–16].

The use of low melting point cathodes (copper melts at 1085 °C compared to graphite which sublimates at 3642 °C) raises a basic question about the operation of the arc, namely how electrons are emitted from the cathode. While this problem has been studied in detail for cathodic arcs [17–21], the arc used in nanosynthesis is an anodic arc and operates in a different regime [22]. Models of the anodic carbon arc [23,22] show that temperatures over 3000 °C are required at the cathode, while experimentally, cathodes remain undamaged during the process.

To explain this discrepancy, the current density at the cathode could be reduced by having the current flow to the entire cathode surface, reducing the temperature required for thermionic emission to support the current, which has been observed in simulations [12]. Alternatively, it has been proposed that the deposit formed during the arc is the source of emission based on its structure after arc operation [24]. This is supported by observations that carbon–copper arcs became carbon–carbon arcs after deposit formation on the

^{*} Corresponding author.

E-mail addresses: jn8@princeton.edu (J. Ng), yraitses@pppl.gov (Y. Raiteses).

<http://dx.doi.org/10.1016/j.carbon.2014.05.007>

0008-6223/© 2014 Elsevier Ltd. All rights reserved.

copper electrode [25]. Similar processes and suggestions about the role of the deposit were also proposed for hydrocarbon arc discharges with copper cathodes [26,27].

In order to determine the source of electrons in the arc and the current distribution at the cathode, we operated the carbon arc using different cathode geometries and materials, including copper and graphite, together with temperature measurements. It is shown that during the steady state operation of the arc, most of the current flows within the area directly across from and of similar size to the anode, and that the formation of the deposit plays an important role in electron emission. In particular, the deposit (1) changes the arc from graphite–copper or graphite–graphite to graphite–deposit and (2) reaches the high temperatures necessary for thermionic emission to provide the electron current. Moreover, the carbon deposit on the cathode (3) reduces the heat flux from the arc plasma to the cathode. This is due to a very low thermal conductivity of the cathode deposit, which was deduced from electrode temperature measurements during the arc experiments. A preliminary material evaluation suggests that the low thermal conductivity of the cathode deposit could be due to its complex morphology and a very low density as compared to graphite and the cathode material.

The main implication of this study is that the formation of the cathode deposit during the arc should be taken into account for self-consistent modelling of the arc discharge for the synthesis of nanomaterials, including, but not limited to, the synthesis of carbon nanostructures such as nanotubes, fullerenes and graphene. As the size of the deposit increases with ablation rate, which determines deposition and hence yield, the inclusion of the deposit in models will be important in regimes favourable for high yield nanosynthesis.

2. Experimental setup

The arc experiments were performed in a helium atmosphere within a 10 inch 6-way cross using the setup shown in Fig. 1, which is similar to that used in Refs. [14,28]. The helium pressure was maintained at 500 Torr using a computer-controlled solenoidal valve. Cylindrical graphite anodes and cathodes of

diameter 6 mm and 12 mm were used, where 6 mm is the typical anode diameter in synthesis experiments [29,5,7]. The copper cathodes had diameters 38 mm and 50 mm.

The position of the anode was controlled by a stepper motor and a potentiometer used to measure the arc voltage, both connected to a data acquisition system. In all the experiments performed, the electrode separation was controlled by maintaining the voltage in the external circuit between 20 V and 25 V as the anode ablated. Discharge current was kept at approximately 65 A. Arcing was initiated by bringing the anode into contact with the cathode, after which the control system would increase the electrode separation until the specified arc voltage was reached. With the 6 mm anode, the voltage remained at approximately 25 V while the voltage during the arc with the 12 mm anode was approximately 21 V. The actual discharge voltage was approximately 20 V for the 6 mm anode arc and 18 V for the 12 mm anode arc after subtracting the resistance of the circuit elements and carbon deposit.

To measure the cathode temperature, a K-type thermocouple was placed 2 mm below the surface of a copper cathode directly opposite the anode. Experiments to measure the deposit temperature used an electrode in which existing cathode deposits to be mounted (Fig. 2(a)), and a C-type thermocouple was placed just below the surface of the deposit. Additionally, a FLIR Tau 640 1.7 infrared camera together with a 3.2% transmittance neutral density filter was used for temperature measurements. Absolute calibration of the camera was performed using arcs between graphite electrodes in conjunction with thermocouple measurements.

For the experiments used to determine the current distribution in the arc, shielded and segmented cathodes were used with 6 mm graphite anodes (Fig. 2(b) and (c)). The shielded copper cathode was covered by an insulating layer of boron–nitride except for a 6 mm diameter opening, while the segmented cathode consisted of an inner region of 6 mm diameter insulated from an outer ring of diameter 50 mm by a 2 mm layer of insulation.

3. Electron emission

We now analyse possible mechanisms of electron emission which could supply the electrons necessary to maintain the current observed in arcs. To do so, we first estimate the electron current fraction by measuring the ablation rates for 65 A arcs, and show that the current cannot be supported by emission from the copper surface. Under the conditions described in the previous section, the arcs operated in the anodic mode with deposit formation on the cathode [14,29]. The results are shown in Table 1 and are consistent with measurements by Fetterman et al. [14]. We found no appreciable difference between the rates for copper and carbon cathodes. The deposits grown were roughly circular with diameter 7–9 mm. With the 6 mm diameter anodes, deposits would grow until the extinguishing of the arc (in this set of experiments the longest was 17 mm), while with the 12 mm diameter anodes deposits did not exceed 1 mm in thickness.

The maximum ion current is estimated by assuming that all the ablated material is singly ionised and delivers current

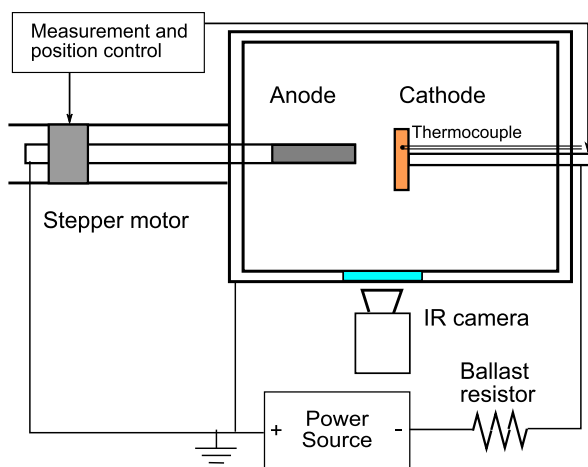


Fig. 1 – Setup used in carbon arc experiments, similar to Ref. [14]. (A colour version of this figure can be viewed online.)

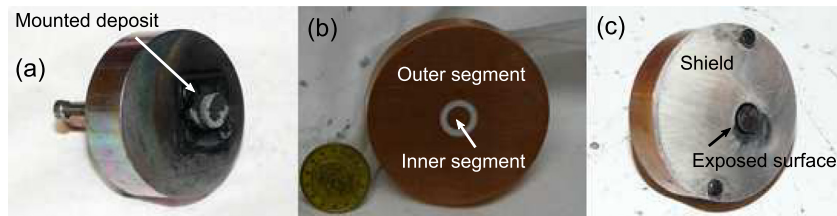


Fig. 2 – Cathodes used in the experiment. (a) Copper cathode with mounted deposit, (b) segmented cathode, (c) shielded cathode. (A colour version of this figure can be viewed online.)

Table 1 – Ablation rates and estimated ion current for a 65 A arc with different cathode materials and anode diameters.

Cathode	Anode diameter (mm)	Ablation (mg/s)	Max ion current (A)
Carbon	12	0.33 ± 0.12	5.2 ± 1.9
Carbon	6	8 ± 2	128 ± 32
Copper	12	0.33 ± 0.08	5.2 ± 1.2
Copper	6	10 ± 2	160 ± 32

to the cathode. To account for current due to evaporation from the cathode and redeposition [30,31], we assume that the evaporation rate at the cathode is less than that at the anode. If all of the evaporated atoms at the cathode were ionised and redeposited, the total ion current would be twice that due to ions from the anode. The resulting current is shown in the final column of Table 1. For the 12 mm anode, an electron current of larger than 60 A would be required to support the arc. For the 6 mm anode, the observed ablation could support the arc current; however, in a typical carbon arc, the ionisation degree is 10^{-3} to 10^{-4} , much less than the 100% assumed here [32]. The ion current would then be reduced to less than 0.12 A, so we would also expect a large electron current for the 6 mm anode.

Supplying this electron current requires electron emission from the cathode, which can take the form of thermo-field emission, secondary emission or photoemission [17,1,33]. In particular, Ref. [33] shows that field emission and various ionisation mechanisms cannot account for the electron current observed in an argon arc with a non-thermionic cathode, and we perform a similar analysis for the carbon arc in helium.

3.1. Thermo-field emission

Heating a solid to high temperatures increases the number of electrons with the energy needed to overcome the work function, while strong electric fields at the surface modify the shape of the potential well. Electron emission due to the combination of these effects is known as thermo-field emission [34,17,35]. A convenient parameterisation of the thermo-field current in units of A/cm² is given by Hantzsche [34]:

$$j_{TF} = k(AT^2 + BE^{9/8}) \exp \left[- \left(\frac{T^2}{C} + \frac{E^2}{D} \right)^{-1/2} \right] \quad (1)$$

where $k = 1.45$, $A = 120$, $B = 406 E^{0.1(\phi-4.5)} \exp(-2.22(\phi-4.5))$, $C = 2.727 \times 10^9 (\phi/4.5)^2$ and $D = 4.252 \times 10^{17} (\phi/4.5)^2$. T is the

temperature in K, E the electric field in V/cm and ϕ the work function in eV. The values of A , B , C and D are from the limiting thermionic and field emission expressions, while k and the functional form are determined by minimising the error in Eq. (1) when compared with numerical calculations [34]. For reference, the work functions of copper and graphite are 4.4 eV and 4.7 eV respectively [1].

With respect to our experiments, the current density was estimated as at least ~ 230 A/cm² for a 65 A arc with an electron current fraction of greater than 0.9, which would require temperatures of above 3200 °C – above the melting point of copper – or electric fields of greater than 10^7 V/cm. If these conditions were to hold, there would be visible damage to the cathode due to melting and/or ablation, which we do not observe, while the typical field at the cathode under these conditions is on the order of 10^5 V/cm [1]. As such, thermo-field emission from the copper cathode cannot account for the observed electron emission during the steady state operation of the arc. Note that during the initial phase of the arc, it operates in the cathodic mode before a transition to the anodic mode which is studied here [32].

3.2. Secondary emission

Electrons are also emitted due to the bombardment of the surface by ions and excited atoms. In the carbon arc, only carbon ions are considered due to helium's high ionisation potential [12], though metastable helium atoms are present and can cause Auger emission [32,36]. At low energies, the secondary electron yield γ_i from ion bombardment depends only on the ionisation energy I and work function ϕ and can be estimated by the empirical formula $\gamma_i = 0.016(I - 2e\phi)$ [1,37]. For carbon ions impacting a copper surface, this is approximately 0.04. Given the ion current fraction of less than 0.1 in our experiment with the 12 mm anode, secondary emission due to ions provides at most 0.2 A for a 65 A arc and cannot be the source of the electrons in the arc.

In Ref. [33], Auger emission due to metastable excited argon atoms the main source of electron current [33]. For helium atoms and copper surfaces, the electron yield is about 1 electron per incident atom [38]. However, due to the higher excitation energies of helium and low arc voltage, the metastable density is too low to provide the required current. The density is found by balancing production by electron excitation against cumulative ionisation [36], given by:

$$n_N n_e C_M^0 = n_M n_e C_M^+ \quad (2)$$

Here n_N is the neutral density, n_e the electron density and n_M is the metastable density. The C 's are rate coefficients which are found by integrating the cross sections for excitation and ionisation with the electron distribution, assumed to be Maxwellian [36]. At an electron temperature of 0.6 eV, the estimated metastable helium density is on the order of 10^{11} m^{-3} , which gives a current of 13 nA assuming thermal flux to the cathode. Auger emission due to carbon is not considered as the metastable 1D and 1S states have energies 1.3 eV and 2.7 eV, below the work functions of copper and graphite of 4.4 eV and 4.7 eV [39,40,1,41].

3.3. Photoemission

To estimate the maximum photoemission from the surface, we assume that at most half of the radiation from the arc reaches the cathode, and a photon energy of 5 eV, the lowest wavelength line of carbon, which gives a yield of 10^{-2} electrons per photon at a copper surface [42,43]. If all of the arc's power were radiated, at most 825 W of radiation would be available for photoemission, which would give a maximum current of approximately 1.7 A. The yield for graphite is approximately 10^{-6} , which would provide 1.7×10^{-4} A [44].

We have thus shown that the above emission mechanisms cannot account for the electron current from a low melting point cathode during an anodic arc. Instead, temperature measurements will reveal that it is the formation of the carbon deposit on the cathode which allows the high temperatures necessary for electron emission to be reached.

4. Current distribution and cathode temperature

To determine if the arc current flows through the entire cathode or just a small region across from the anode, experiments with shielded and segmented cathodes were performed. In the experiment with the shielded cathode, a carbon deposit formed over the unshielded area, after which the arc continued to operate with the entire current flowing through the cathode deposit. With the segmented cathode, at most 4 A flowed through the outer segment during a 65 A arc. At lower currents, no current in the outer segment was observed. This shows that most of the current flows through the small central region directly opposite the anode. As such, the observed current density is over 230 A/cm^2 . The observation that the arc operates between the deposit and anode is also consistent with Upson's [25] observations that the copper–carbon arc becomes the carbon–carbon arc after deposit formation.

The variation of copper cathode temperature with time for arcs with 12 mm and 6 mm diameter anodes respectively is shown in Fig. 3. The highest temperature measured in the copper electrode was $1000 \pm 20^\circ\text{C}$ during the experiment with the larger anode, which is still below the melting point of copper of 1085°C . This was due to the cathode deposit being thinner, so that the thermocouple was in closer proximity to the actual cathode surface. Also of note in Fig. 3(b) is the extinguishing of the arc around $t = 100$ s and re-ignition at $t = 120$ s, caused by the deposit becoming detached from the cathode and falling off. Immediately after re-ignition, the rate

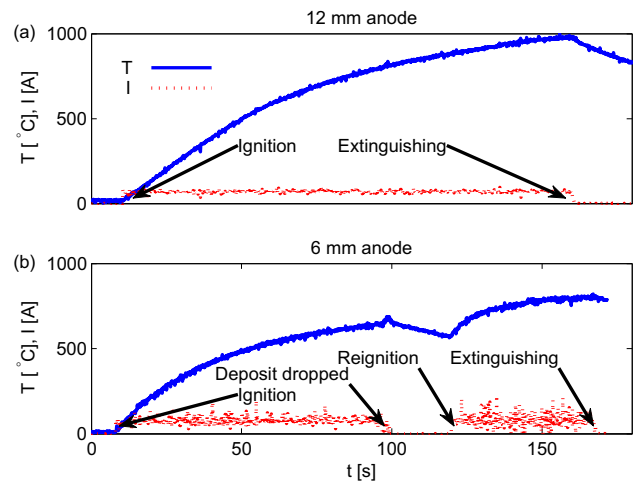


Fig. 3 – Cathode temperature and discharge current during the operation of arcs with (a) 12 mm and (b) 6 mm anodes. The thermocouple was placed 2 mm below the cathode surface exposed to the arc. (A colour version of this figure can be viewed online.)

of increase of temperature was larger than just before $t = 100$ s, showing that the presence of the deposit reduces heat flux to the cathode. These observations show that the deposit is a critical element in the operation of the arc.

Fig. 4 shows infrared images of the electrodes during an arc between 12 mm diameter anodes and graphite and copper cathodes. During both arcs, small deposits formed on the cathode, and the highest surface temperature was $(3500 \pm 200) \text{ K}$, with a larger region where temperatures were over 3100 K. The uncertainties in the temperature measurements are due to the extrapolation of the calibration curve. Thermocouple readings within the deposit were consistent with the infrared measurements and exceeded 2593 K, the

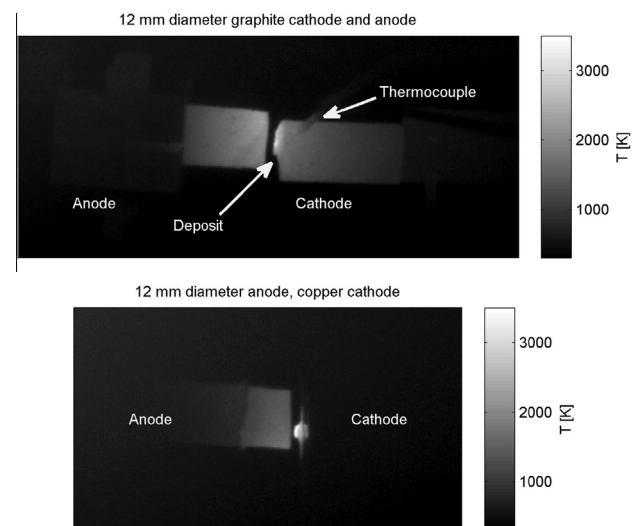


Fig. 4 – Top: infrared camera image of electrodes during an arc discharge between two 12 mm graphite electrodes. Bottom: electrodes during arc between 12 mm graphite anode and copper cathode.

maximum temperature which can be measured by C-type thermocouples. Data for 6 mm diameter anodes are not available due to the growth of the “collar” around the deposit preventing a clear view of its surface from being obtained. These results show that the deposit reaches the high temperatures necessary for thermionic emission to provide the electron current in the arc, in agreement with observations of the deposit structure after the arc [24]. Within the observed surface temperature range, the thermo-field emission current is between 60 A/cm² and 500 A/cm², with most of the contribution being thermionic. This would supply at least a quarter to all of the current in the arc.

The deposit is thus the source of electron emission and is effectively the cathode, meaning that the arc should not be considered graphite–copper, but graphite–carbon deposit [25,24]. This also explains why the cathode remains undamaged, as the deposit reduces heat flux to the copper surface, as seen earlier in Fig. 3(b). Apparently, the carbon deposit acts here as a thermal insulator.

The known conductivity value for graphite is approximately 13 W/m/K above 2500 °C [45], which is already lower than that of copper, which is over 300 W/m/K above 1000 °C [46]. It is known from previous work on Raman spectroscopy of carbon arc deposits [28] and also shown in the following section for the deposits obtained in this work that their structures and properties are different from graphite. This may imply that thermal conductivity of the carbon deposit can be different from graphite. While data are not available, the upper image in Fig. 4 with the graphite–graphite arc shows that it is lower than that of graphite based on the different temperature gradients in the deposit and graphite regions. From our experiments, the estimated thermal conductivity is 1–2 W/m/K, which is not unusual for carbonaceous products [47]. Our estimate here does not include the effects of convective and radiative cooling. These additional cooling mechanisms would effectively increase the observed conductivity of the deposit, and as such, the value of thermal conductivity we determined is likely an overestimate. For example, the addition of radiative cooling would increase heat loss from the sides of the deposit by a term proportional to T^4 , which would cause a steeper temperature gradient to exist in the deposit than if there were conductivity alone.

In previous works on hydrocarbon arcs with deposit formation, the low thermal conductivity has been attributed to contact resistance between the deposit and copper [27], but this is not necessary as the thermal conductivity of amorphous hydrocarbons can be low. For example, the thermal conductivity of hydrogenated amorphous carbon films is 1 W/m/K [47]. Furthermore, in our work, the large temperature gradient is also observed in the graphite–graphite arc where there is good contact between the deposit and cathode.

The results of our experiments reveal that the arc current flows through a small region opposite the anode and that thermionic emission is the source of electron emission during the anodic arc and explain how the high temperatures required for this process are reached without damaging the low-melting point cathode material. Due to the measured low heat conductivity of the deposit, the high temperatures at the surface exposed to the arc required to support emission can exist without the cathode reaching its melting

temperature. It should also be emphasized that the deposit also forms in experiments with graphite cathodes, meaning that the role of the deposit in the arc described here is more general and not exclusive to arcs with low melting point cathodes. Thus, after the formation of the deposit, the arc is not between the graphite anode and the cathode material, but is a graphite-cathode deposit arc. With respect to nanosynthesis, the growth of single-walled nanotubes mainly takes place on the periphery of the deposit [13,5,12], away from the region where the current flows, implying that the cathode material not covered by the deposit (in our case copper) is important in their formation [7].

5. Carbon deposit on the cathode surface

A preliminary ex-situ characterization of the cathode deposits was conducted for the arc discharges with 6 mm and 12 mm diameter anodes and with the copper cathode. The deposits were collected after the arc discharge. Then, their dimensions and weight were measured to estimate the density. For different anodes, the cathode deposits had different dimensions (Fig. 5) and densities. For example, the density of the deposit formed with the 6 mm anode was 1.34 ± 0.06 g/cm³. This is smaller than the density of the graphite 2.09 g/cm³ but comparable with the density of graphite-like amorphous carbon, 1.2–1.5 g/cm³ [48]. For the 12 mm diameter anode, the measured density was even smaller $\sim 0.8 \pm 0.2$ g/cm³. These density results correlate with the above results for the thermal conductivity obtained for different anodes and graphite. In particular, smaller densities of the cathode carbon deposits as compared to graphite correlate with their lower thermal conductivity measured in these experiments.

A FEI XL30 FEG-SEM field emission high resolution scanning electron microscope (SEM) was used for structural evaluation of the cathode deposits. This SEM is equipped with an EVEX Energy-dispersive X-ray spectroscopy (EDS) system to provide a high-resolution two-dimensional elemental distribution map of the deposit surface. For all deposits, carbon was the only element detected by the EDS system. Evaluation

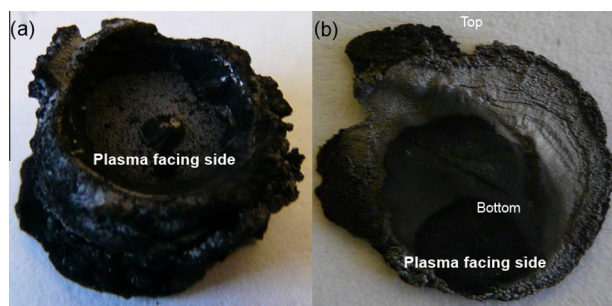


Fig. 5 – Carbon deposits removed from the cathode after a 65 A arc discharge was run for about 1 min: (a) about 8 mm diameter and 5 mm height deposit from the arc discharge with a 6 mm diameter anode; (b) about 9 mm diameter and 0.6 mm height deposit from the arc discharge with a 12 mm diameter anode. (A colour version of this figure can be viewed online.)

of SEM images (Fig. 6) revealed that all deposits have an inhomogeneous porous morphology consisting of spherical, flat, tubular and chain-like particles of different nano and micro sizes. Similar types of particles were also obtained in other carbon arc discharges [49–51,24]. Spatial variation of deposit morphology is very complex and requires a detailed analysis. This is beyond the scope of this paper, which is focused on the role of the deposit in the current conduction between the arc and the cathode and the thermal insulation of the cathode from the plasma.

It is known that for carbon materials, such as carbon black and coal ash, the grain size and porosity can strongly affect the thermal conductivity of these materials [52,53]. In particular, the thermal conductivity decreases with the porosity, but increases with the grain size. We could not detect a reliable and reproducible correlation between the size of the microstructures, particularly for spherical particles (Fig. 6), and the cathode deposits produced with the 6 mm and 12 mm anodes. Spherical morphology was dominant for the plasma-facing surfaces of both deposits (Fig. 6), but sphere sizes varied for different runs with the same anode diameters. On the opposite surfaces of the deposits facing the copper cathode, morphology was different, consisting of tubular and chain-like particles. From a visual evaluation of SEM images, the cathode deposit formed with the smaller 6 mm anode appears to be less porous (Fig. 6) than the deposit obtained with the larger anode. A somewhat similar observation was obtained for the interiors of both deposits. Thus, the thinner deposit formed with the 12 mm anode would be expected to have a lower conductivity than the larger deposit formed using the 6 mm anode, which would support the

larger temperature gradient between the emitting surface and the copper. This hypothesis requires a more comprehensive validation.

Complex structural variations of the deposits were also detected with Raman spectroscopy (Fig. 7) using a Horiba Scientific LabRam HR800 μ -Raman system. During all the Raman spectra measurements, the power of the green laser (wavelength 532 nm) at the deposits was kept very low at about 3 mW. For nearly all deposits and different locations within the deposits the Raman spectra display two typical peaks at 1340 cm^{-1} and 1590 cm^{-1} , which correspond to the D and G bands respectively.

The G-band is associated with the first-order scattering of the E_{2g} mode observed for sp^2 carbon domains, while the pronounced D-band is disordered band associated with local defects and disorders, particularly the defects located at the edges of graphene and graphite platelets [54]. Higher disorder in graphite leads to a broader D-band of higher intensity as compared to the intensity of the G-band. Therefore, the intensity ratio of D-band to G-band (I_D/I_G) is usually used as a measure of the disorder. It appears from Fig. 7 that for different spots on different sides of both deposits, there are different I_D/I_G values, indicating the crystal quality changes with the location. Because the I_D/I_G values obtained for the deposit from the arc with the 12 mm anode are generally higher than the I_D/I_G values for the deposit obtained with the smaller anode, the deposit from the arc with the larger anode appears to have more disordered structure. Furthermore, for each deposit, the plasma-facing side has generally a fewer defects because the ratio I_D/I_G is lower than the cathode-facing side. These observations seem to be consistent with results of

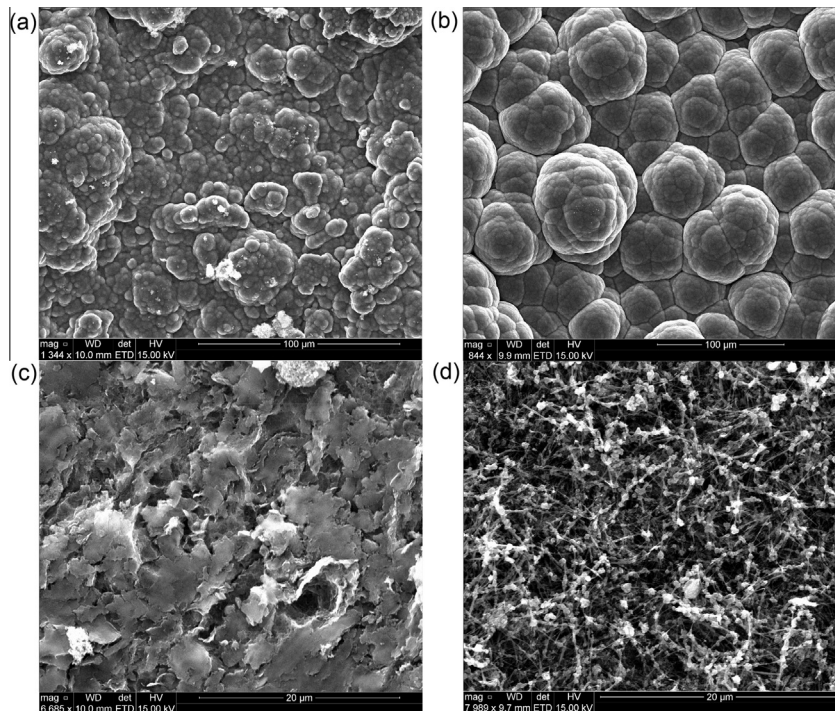


Fig. 6 – Examples of SEM images of the cathode deposits obtained in the arc discharge with different graphite anodes. (a) and (b) From the plasma-facing surfaces of the 6 and 12 mm anodes respectively. (c) and (d) From the cathode-facing surfaces of the same deposits.

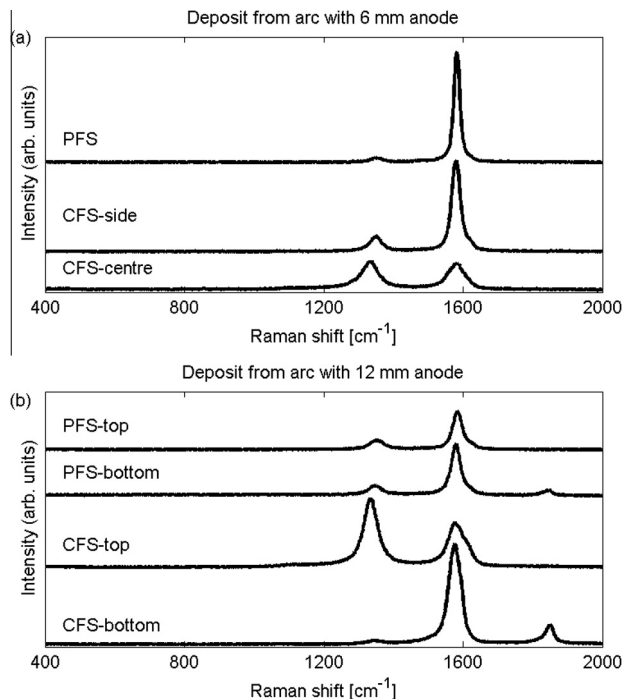


Fig. 7 – Raman spectra of the cathode deposits. (a) Arc with the 6 mm anode and (b) arc with the 12 mm anode. For each deposit, the measurements were conducted at different locations of the plasma-facing side (PFS) and the cathode facing side (CFS). Centre, top and bottom refer to different locations of the deposits shown in Fig. 5.

SEM evaluation, which pointed to strong differences between opposite sides of the same deposit.

Interestingly, for the deposit obtained for the 12 mm anode, Raman spectra have a scattering peak at 1850 cm^{-1} on both plasma-facing and cathode-facing sides of this deposit (Fig. 7(b)). In Ref. [55], a similar peak was observed for cathode deposits of the carbon arc discharge in a hydrogen atmosphere. This peak was attributed to carbon nanowires formed in multiwalled carbon nanotubes formed on the cathode. Tubular structures were also observed in this work (Fig. 6(d)), but no transmission electron microscopy studies were conducted to identify their detailed structure or the presence of one-dimensional carbon chains such as nanowires.

Finally, Fig. 8 compares X-ray diffraction (XRD) patterns measured for the cathode deposits and the graphite material of the anode before its exposure to the plasma. XRD measurements were conducted using a Rigaku MiniFlex XRD/X-ray diffractometer ($\lambda = 1.5406\text{ \AA}$). The data was processed with X-ray Powder Diffraction Software PDXL. Measured XRD patterns show characteristic peaks of a typical hexagonal structure. Analysis of diffraction peaks, including calculation of lattice parameters, crystalline sizes, and the diffraction angle was conducted using a standard procedure for carbon materials described elsewhere [56].

For the (002), (100) and (004) diffraction peaks, the lattice constant, interplanar distance and crystallite size of both deposits increased as compared to the graphite material of the anode. In addition, for the deposits, the (002) and (004)

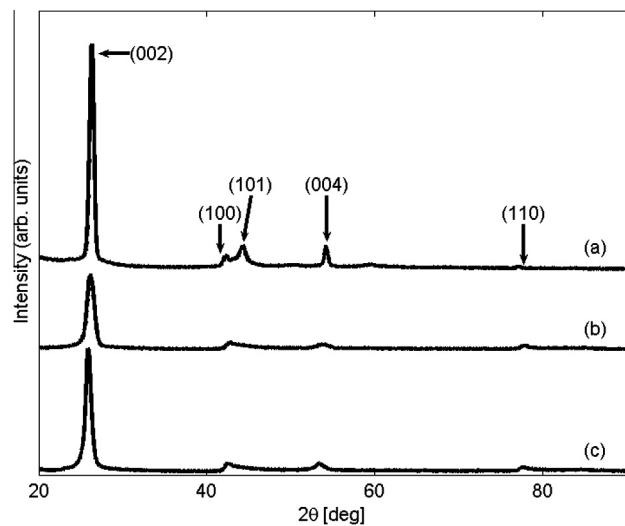


Fig. 8 – X-ray diffraction patterns of the (a) graphite material before the exposure to the plasma, (b) the cathode deposit obtained for the arc with the 6 mm diameter anode and (c) the cathode deposit obtained for the 12 mm diameter anode.

diffraction peaks are shifted to lower angles. For example, for graphite and the deposits from the arcs with the 6 mm and 12 mm anodes, $d_{002} = 0.3382\text{ nm}$, 0.3406 nm and 0.3443 nm at $2\theta = 26.33^\circ$, 26.14° and 25.86° , respectively. A qualitatively similar trend was also observed for the (004) diffraction peak. Refs. [57,26] observed similar behavior for graphite before arc evaporation and deposits produced by arc discharge. Larger interlayer spacing of carbon deposits was attributed to the turbostratic structure of carbon nanotubes and nanofibers. This may be consistent with the reported SEM observation of tubular structures for the deposit obtained with the 12 mm anode (Fig. 6(d)) and measured Raman spectra for this deposit (Fig. 7(b)).

The material analysis shows that the deposit has a complex and inhomogeneous structure, with spherical morphology observed on the plasma facing surface and tubular and chain like structures on the copper facing surface. These observations are supported by Raman, SEM and XRD data. The porosity and lower density of the deposit as compared to graphite is consistent with the lower thermal conductivity estimated from our experiments.

6. Conclusion

To summarise, anodic arc experiments were conducted between graphite anodes and graphite and copper cathodes. Using 6 mm diameter graphite anodes, which is typical for nanosynthesis [5,13], all of the current was found to flow through the deposit formed on the region of the cathode directly opposite the anode, and the current was largely due to electrons. The formation of the cathode deposit is essential in the sustaining of the arc during steady state operation as it allows the high temperatures necessary for thermionic emission to provide the electron current in the arc to exist without damaging the cathode. In addition, it changes the arc from a

graphite-cathode to a graphite-deposit arc. The results support phenomenological descriptions of the role of the deposit in Refs. [24,25].

Analysis of the deposits using SEM, Raman spectroscopy and XRD revealed complex inhomogeneous morphologies and more porous structures with lower densities as compared to the original graphite electrode material. This could be the cause of the lower thermal conductivities observed but requires further theoretical and experimental confirmation.

The important practical implication of this work is that self-consistent models of the arc discharge for nanosynthesis, including, but not limited to, carbon and boron nitride nanotubes and fullerenes, need to account the important role of the cathode deposit in the sustaining the arc discharge.

Acknowledgements

We would like to thank Dr. Zhaofeng Wu, Mr. Yao-Wen Yeh and Dr. Nan Yao for assistance with material evaluation and fruitful discussions of the deposit structure. We also thank Mr. Alex Merzhevskiy, Mr. Enrique Merino for technical support, Dr. Travis Gray for assisting with infrared measurements, and Dr. Michael Keidar and Mr. Emre Türköz for fruitful discussions of arc physics. This work was supported by DOE contract DE-AC02-09CH11466.

REFERENCES

- [1] Raizer Y. *Gas discharge physics*. Springer-Verlag; 1991.
- [2] Null MR, Lozier WW. Carbon arc as a radiation standard. *J Opt Soc Am* 1962;52(10):1156–61. <http://dx.doi.org/10.1364/JOSA.52.001156>. URLhttp://www.opticsinfobase.org/abstract.cfm?URI=josa-52-10-1156.
- [3] Null MR, Lozier WW. Carbon arc image furnaces. *Rev Sci Instrum* 1958;29(2):163–70. <http://dx.doi.org/10.1063/1.1716128>. URLhttp://link.aip.org/link/?RSI/29/163/1.
- [4] Iijima S et al. Helical microtubules of graphitic carbon. *Nature* 1991;354(6348):56–8.
- [5] Journet C, Maser W, Bernier P, Loiseau A, De La Chapelle ML, Lefrant dIS, et al. Large-scale production of single-walled carbon nanotubes by the electric-arc technique. *Nature* 1997;388(6644):756–8.
- [6] Mansour A, Razafinimanana M, Monthieux M, Pacheco M, Gleizes A. A significant improvement of both yield and purity during {SWCNT} synthesis via the electric arc process. *Carbon* 2007;45(8):1651–61. <http://dx.doi.org/10.1016/j.carbon.2007.03.044>. URLhttp://www.sciencedirect.com/science/article/pii/S0008622307001522.
- [7] Colbert DT, Zhang J, McClure SM, Nikolaev P, Chen Z, Hafner JH, et al. Growth and sintering of fullerene nanotubes. *Science* 1994;266(5188):1218–22. <http://dx.doi.org/10.1126/science.266.5188.1218>. URLhttp://www.sciencemag.org/content/266/5188/1218.abstract.
- [8] Keidar M, Shashurin A, Li J, Volotskova O, Kundrapu M, Zhuang TS. Arc plasma synthesis of carbon nanostructures: where is the frontier? *J Phys D Appl Phys* 2011;44(17):174006. URLhttp://stacks.iop.org/0022-3727/44/i=17/a=174006.
- [9] Baughman RH, Zakhidov AA, de Heer WA. Carbon nanotubes – the route toward applications. *Science* 2002;297(5582):787–92. <http://dx.doi.org/10.1126/science.1060928>. URLhttp://www.sciencemag.org/content/297/5582/787.abstract.
- [10] Thostenson ET, Ren Z, Chou TW. Advances in the science and technology of carbon nanotubes and their composites: a review. *Comp Sci Technol* 2001;61(13):1899–912. [http://dx.doi.org/10.1016/S0266-3538\(01\)00094-X](http://dx.doi.org/10.1016/S0266-3538(01)00094-X). URLhttp://www.sciencedirect.com/science/article/pii/S026635380100094X.
- [11] Meyyappan M. *Carbon nanotubes: science and applications*. CRC press; 2004.
- [12] Kundrapu M, Keidar M. Numerical simulation of carbon arc discharge for nanoparticle synthesis. *Phys Plasmas* 2012;19(7):073510. <http://dx.doi.org/10.1063/1.4737153>. pages 9. URLhttp://link.aip.org/link/?PHP/19/073510/1.
- [13] Ostrogorsky A, Marin C. Heat transfer during production of carbon nanotubes by the electric-arc process. *Heat Mass Transfer* 2006;42:470–7. <http://dx.doi.org/10.1007/s00231-005-0644-7>. URLhttp://dx.doi.org/10.1007/s00231-005-0644-7.
- [14] Fetterman AJ, Raitses Y, Keidar M. Enhanced ablation of small anodes in a carbon nanotube arc plasma. *Carbon* 2008;46(10):1322–6. <http://dx.doi.org/10.1016/j.carbon.2008.05.018>. URLhttp://www.sciencedirect.com/science/article/pii/S0008622308002418.
- [15] Chopra NG, Benedict LX, Crespi VH, Cohen ML, Louie SG, Zettl A. Fully collapsed carbon nanotubes. *Nature* 1995;377:135.
- [16] Keidar M, Levchenko I, Arbel T, Alexander M, Waas AM, Ostrikov KK. Increasing the length of single-wall carbon nanotubes in a magnetically enhanced arc discharge. *Appl Phys Lett* 2008;92(4):043129. <http://dx.doi.org/10.1063/1.2839609>. pages 3. URLhttp://link.aip.org/link/?APL/92/043129/1.
- [17] Anders A. *Cathodic arcs: from fractal spots to energetic condensation*. Springer; 2008.
- [18] Jüttner B. Cathode spots of electric arcs. *J Phys D Appl Phys* 2001;34(17):R103. URLhttp://stacks.iop.org/0022-3727/34/i=17/a=202.
- [19] Meunier JL, Coulombe S. Cold cathode arc attachment: the importance of the high local pressure. *Pure Appl Chem* 1998;70(6):1175–80.
- [20] Hantzschke E. - theories of cathode spots. In: Boxman RL, Sanders DM, Martin PJ, editors. *Handbook of vacuum arc science and technology*. Park Ridge, NJ: William Andrew Publishing; 1996. p. 151–208. <http://dx.doi.org/10.1016/B978-081551375-9.50007-2>. ISBN 978-0-8155-1375-9. URLhttp://www.sciencedirect.com/science/article/pii/B9780815513759500072.
- [21] Benilov MS, Marotta A. A model of the cathode region of atmospheric pressure arcs. *J Phys D Appl Phys* 1995;28(9):1869. URLhttp://stacks.iop.org/0022-3727/28/i=9/a=015.
- [22] Alekseyev N, Dyuzhev G. Arc discharge with a vaporizable anode: Why is the fullerene formation process affected by the kind of buffer gas? *Tech Phys* 2001;46(10):1247–55. <http://dx.doi.org/10.1134/1.1412058>. URLhttp://dx.doi.org/10.1134/1.1412058.
- [23] Keidar M, Beilis II. Modeling of atmospheric-pressure anodic carbon arc producing carbon nanotubes. *J Appl Phys* 2009;106(10):103304. <http://dx.doi.org/10.1063/1.3262626> (pages 6). URLhttp://link.aip.org/link/?JAP/106/103304/1.
- [24] Tang D, Sun L, Zhou J, Zhou W, Xie S. Two possible emission mechanisms involved in the arc discharge method of carbon nanotube preparation. *Carbon* 2005;43(13):2812–6. <http://dx.doi.org/10.1016/j.carbon.2005.05.034>. URLhttp://www.sciencedirect.com/science/article/pii/S0008622305003167.
- [25] Upton WL. Observations on the electric arc. *Proc Phys Soc London* 1907;21(1):1. URLhttp://stacks.iop.org/1478-7814/21/i=1/a=301.

- [26] Fridlyand MG, Nemoitin NA, Koss VA. Cathode processes formed in a condensed arc in a hydrocarbon. *High Temp* 1976;14(1):19–22.
- [27] Zhukov MF, Pustogarov AV, Dandaron GNB, Timoshevskij AN. Thermochemical cathodes (Novosibirsk: Nauka) in Russian 1980.
- [28] Raitse Y, Skinner C, Jiang F, Duffy T. Raman spectroscopy of carbon dust samples from {NSTX}. *J Nucl Mater* 2008;375(3):365–9. <http://dx.doi.org/10.1016/j.jnucmat.2008.01.012>. URLhttp://www.sciencedirect.com/science/article/pii/S0022311508000445.
- [29] Shashurin A, Keidar M. Factors affecting the size and deposition rate of the cathode deposit in an anodic arc used to produce carbon nanotubes. *Carbon* 2008;46(13):1826–8. <http://dx.doi.org/10.1016/j.carbon.2008.08.002>. URLhttp://www.sciencedirect.com/science/article/pii/S0008622308004065.
- [30] Beilis I. Kinetics of plasma particles and electron transport in the current-carrying plasma adjacent to an evaporating and electron emitting wall. *IEEE Trans Plasma Sci* 2006;34(3):855–66. <http://dx.doi.org/10.1109/TPS.2006.873250>.
- [31] Puchkarev VF, Chesnokov SM. Erosion rate and voltage distribution in contracted (with cathode spot) and diffuse (spotless) low-current vacuum arcs. *J Phys D Appl Phys* 1992;25(12):1760. URLhttp://stacks.iop.org/0022-3727/25/i=12/a=011.
- [32] Shashurin A, Li J, Zhuang T, Keidar M, Beilis II. Application of electrostatic langmuir probe to atmospheric arc plasmas producing nanostructures. *Phys Plasmas* 2011;18(7):073505. <http://dx.doi.org/10.1063/1.3614538> (pages 7). URLhttp://link.aip.org/link/?PHP/18/073505/1.
- [33] Lowke J, Tanaka M. The physics of non-thermionic cathodes of electric arcs. In: Gas discharges and their applications, 2008. GD 2008. 17th International conference on. 2008, p. 137–140.
- [34] Hantzsche E. The thermo-field emission of electrons in arc discharges. *Beitrage aus der Plasmaphysik* 1982;22(4):325–46. <http://dx.doi.org/10.1002/ctpp.19820220403>. URLhttp://dx.doi.org/10.1002/ctpp.19820220403.
- [35] Murphy EL, Good RH. Thermionic emission, field emission, and the transition region. *Phys Rev* 1956;102:1464–73. <http://dx.doi.org/10.1103/PhysRev.102.1464>. URLhttp://link.aps.org/doi/10.1103/PhysRev.102.1464.
- [36] Korzec D, Talukder MR, Kando M. Determination of metastable atom concentration by use of electrostatic probe technique. *Sci Technol Adv Mater* 2001;2(3–4):595. URLhttp://iopscience.iop.org/1468-6996/2/3-4/A22.
- [37] Cawthron E. Secondary electron emission from solid surfaces bombarded by medium energy ions. *Aust J Phys* 1971;24(4):859–70.
- [38] Dunning FB, Smith ACH. Secondary electron ejection from metal surfaces by metastable atoms. ii. measurements of secondary emission coefficients using a gas cell method. *J Phys B At Mo Phys* 1971;4(12):1696. URLhttp://stacks.iop.org/0022-3700/4/i=12/a=018.
- [39] Skell PS, Engel RR. Reactions of carbon vapor. ii. reactions of ground-state (3p) atomic carbon with olefins 1,2. *J Am Chem Soc* 1966;88(16):3749–58. <http://dx.doi.org/10.1021/ja00968a014>. URLhttp://pubs.acs.org/doi/abs/10.1021/ja00968a014.
- [40] Freund RS. Dissociation by electron impact of oxygen into metastable quintet and long-lived high-rydberg atoms. *J Chem Phys* 1971;54(7):3125–41. <http://dx.doi.org/10.1063/1.1675301>. URLhttp://scitation.aip.org/content/aip/journal/jcp/54/7/10.1063/1.1675301.
- [41] Salmi LA. Theory of spin polarization in the metastable-hemetal interaction. *Phys Rev B* 1992;46:4180–91. <http://dx.doi.org/10.1103/PhysRevB.46.4180>. URLhttp://link.aps.org/doi/10.1103/PhysRevB.46.4180.
- [42] Berglund CN, Spicer WE. Photoemission studies of copper and silver: experiment. *Phys Rev* 1964;136:A1044–64. <http://dx.doi.org/10.1103/PhysRev.136.A1044>. URLhttp://link.aps.org/doi/10.1103/PhysRev.136.A1044.
- [43] Kramida A, Ralchenko Y, Reader J, NIST ASD Team. NIST atomic spectra database (version 50) 2012; URLhttp://physics.nist.gov/asd.
- [44] Taft E, Apker L. Photoelectric emission from polycrystalline graphite. *Phys Rev* 1955;99:1831–2. <http://dx.doi.org/10.1103/PhysRev.99.1831>. URLhttp://link.aps.org/doi/10.1103/PhysRev.99.1831.
- [45] Powell RW, Schofield FH. The thermal and electrical conductivities of carbon and graphite to high temperatures. *Proc Phys Soc* 1939;51(1):153. URLhttp://stacks.iop.org/0959-5309/51/i=1/a=317.
- [46] Powell RW, Ho CY, Liley PE. Thermal conductivity of selected materials. *Natl Stand Ref Data Ser – Natl Bureau Stand* 1966:8.
- [47] Hurler W, Pietralla M, Hammerschmidt A. Determination of thermal properties of hydrogenated amorphous carbon films via mirage effect measurements. *Diamond Relat Mater* 1995;4(7):954–7. [http://dx.doi.org/10.1016/0925-9635\(94\)00259-2](http://dx.doi.org/10.1016/0925-9635(94)00259-2). URLhttp://www.sciencedirect.com/science/article/pii/S0925963594002592.
- [48] Silva, S.R.P. Microstructure of a-c. In: Silva, S.R.P., editor. Properties of amorphous carbon, EMIS Datareviews Series 29. INSPEC; 2003.
- [49] Guilin Z, Yuedong M, Kingsheng S, Shidong F. Characterization of carbon deposits formed during plasma pyrolysis of xinjiang candle coal. *Plasma Sci Technol* 2009;11(4):487. URLhttp://stacks.iop.org/1009-0630/11/i=4/a=25.
- [50] Liu X, Hong R, Feng W, Badami D. Synthesis of structure controlled carbon nanomaterials by {AC} arc plasma process. *Powder Technol* 2014;256(0):158–65. <http://dx.doi.org/10.1016/j.powtec.2014.01.096>. URLhttp://www.sciencedirect.com/science/article/pii/S0032591014001314.
- [51] Zhao S, Hong R, Luo Z, Lu H, Yan B. Carbon nanostructures production by ac arc discharge plasma process at atmospheric pressure. *J Nanomater* 2011:346206.
- [52] Khizhnyak P, Chechetkin A, Glybin A. Thermal conductivity of carbon black. *J Eng Phys* 1979;37(3):1073–5. <http://dx.doi.org/10.1007/BF00861683>. URLhttp://dx.doi.org/10.1007/BF00861683.
- [53] Rezaei H, Gupta R, Bryant G, Hart J, Liu G, Bailey C, et al. Thermal conductivity of coal ash and slags and models used. *Fuel* 2000;79(13):1697–710. [http://dx.doi.org/10.1016/S0016-2361\(00\)00033-8](http://dx.doi.org/10.1016/S0016-2361(00)00033-8). URLhttp://www.sciencedirect.com/science/article/pii/S0016236100000338.
- [54] Ferrari AC, Robertson J. Interpretation of raman spectra of disordered and amorphous carbon. *Phys Rev B* 2000;61:14095–107. <http://dx.doi.org/10.1103/PhysRevB.61.14095>. URLhttp://link.aps.org/doi/10.1103/PhysRevB.61.14095.
- [55] Zhao X, Ando Y, Jinno M, Suzuki T. Carbon nanowire made of a long linear carbon chain inserted inside a multiwalled carbon nanotube. *Phys Rev Lett* 2003;90:187401. <http://dx.doi.org/10.1103/PhysRevLett.90.187401>. URLhttp://link.aps.org/doi/10.1103/PhysRevLett.90.187401.
- [56] Iwashita N, Park CR, Fujimoto H, Shiraiishi M, Inagaki M. Specification for a standard procedure of X-ray diffraction measurements on carbon materials. *Carbon* 2004;42(4):701–14. <http://dx.doi.org/10.1016/j.carbon.2004.02.008>. URLhttp://www.sciencedirect.com/science/article/pii/S0008622304001046.
- [57] Saito Y, Yoshikawa T, Bandow S, Tomita M, Hayashi T. Interlayer spacings in carbon nanotubes. *Phys Rev B* 1993;48:1907–9. <http://dx.doi.org/10.1103/PhysRevB.48.1907>. URLhttp://link.aps.org/doi/10.1103/PhysRevB.48.1907.